

# An Adaptive Mixer Allocation Algorithm for the Quantum Alternating Operator Ansatz

Xiao-Hui Ni,<sup>1,2</sup> Yu-Sen Wu,<sup>3</sup> Bin-Bin Cai,<sup>4</sup> Wen-Min Li,<sup>1</sup> Su-Juan Qin,<sup>1,\*</sup> and Fei Gao<sup>1</sup>

<sup>1</sup>*State Key Laboratory of Networking and Switching Technology,  
Beijing University of Posts and Telecommunications, Beijing 100876, China*

<sup>2</sup>*School of Cyberspace Security, Beijing University of Posts and Telecommunications, Beijing, 100876, China*

<sup>3</sup>*School of Artificial Intelligence, Beijing Normal University, Beijing 100875, China*

<sup>4</sup>*College of Computer and Cyber Security, Fujian Normal University, Fuzhou ,350117, China*

(Dated: December 30, 2024)

Recently, Hadfield et al. proposed the quantum alternating operator ansatz algorithm (QAOA+), an extension of the quantum approximate optimization algorithm (QAOA), to solve constrained combinatorial optimization problems (CCOPs). Compared with QAOA, QAOA+ enables the search for optimal solutions within a feasible solution space by encoding problem constraints into the mixer Hamiltonian, thus reducing the search space and eliminating the possibility of yielding infeasible solutions. However, QAOA+ may require substantial gates and circuit depth when the mixer is applied to all qubits in each layer, and the implementation cost of the mixer is high. To address these challenges, we propose the adaptive mixer allocation (AMA) algorithm. AMA constructs a feasible space by selectively applying the mixer to partial qubits in each layer based on the evolution of the optimization process. The performance of AMA in solving the maximum independent set (MIS) problem is investigated. Numerical simulation results demonstrate that, under the same number of optimization runs, AMA achieves a higher optimal approximation ratio—1.82% (3.02%) higher than QAOA+ on ER (3-regular) graphs. Additionally, AMA significantly reduces the resource consumption, achieving only 34.08% (29.77%) of QAOA+ circuit depth and 15.05% (18.72%) of the number of CNOT gates, respectively, on ER (3-regular) graphs. These results highlight the ability of AMA to enhance computational efficiency and solution quality, making it particularly valuable for resource-constrained quantum devices.

## I. INTRODUCTION

With advancements in quantum computing technology, many quantum algorithms have been proposed to solve important problems, such as unstructured database search [1], prime factorization [2], and solving systems of linear equations [3]. However, due to the hardware limitations of current noisy intermediate-scale quantum (NISQ) devices, such as limited qubit numbers and high error rates, these algorithms face significant challenges in being efficiently implemented on existing quantum hardware [4]. To better harness the computational power offered by current NISQ devices, quantum-classical hybrid algorithms have been developed, combining the strengths of both quantum and classical computing [5–13].

The quantum approximate optimization algorithm (QAOA) [14–17] is a representative quantum-classical hybrid algorithm and has been widely applied to solve various combinatorial optimization problems (COPs) [18–26]. When solving the constrained COPs (CCOPs), QAOA tends to encode the problem constraints into the target Hamiltonian utilizing the penalty terms [22, 23, 26–28], and then search for the optimal solution using a parameterized quantum circuit (PQC). However, this approach may lead to infeasible solutions (i.e., the solution

violates one or more problem constraints), as QAOA explores the entire Hilbert space, which includes both feasible and infeasible solutions [29].

To address this issue, Hadfield et al. [30] proposed a novel quantum alternating operator ansatz algorithm (QAOA+). QAOA+ constructs a feasible solution space by encoding the problem constraints into the mixer Hamiltonian and searches for the optimal solution within this space [29]. This approach reduces the search space and eliminates the possibility of yielding infeasible solutions [31]. Leveraging these advantages, QAOA+ has been widely utilized to solve various problems [31–37]. However, QAOA+ may require a large number of quantum gates and deep circuit depth, especially when the mixer is applied to all qubits in implementing each layer of the mixer unitary operation, and the implementation overhead of each mixer is costly [33, 38, 39]. Such high resource demands limit the size and complexity of problems that can be addressed on current NISQ devices.

In this paper, we propose an adaptive mixer allocation (AMA) algorithm to reduce the number of quantum gates and the circuit depth overhead. The core idea of the AMA algorithm is to construct a feasible solution space by selectively applying the mixer to partial qubits in each layer based on the evolution of the optimization process, and then to search for the optimal solution within this space. We investigate the performance of the AMA algorithm in solving the maximum independent set (MIS) problem on ER and 3-regular graphs of varying sizes. The MIS problem is an important CCOP that arises in

\* qsujuan@bupt.edu.cn

various fields such as network design, scheduling, and social network analysis, equivalent to the minimum vertex cover or finding a maximum clique of the complementary graph. Additionally, its performance was compared with QAOA+ and two other intuitive algorithms of assigning the mixer, which involved randomly selecting partial qubits for each layer, with either uniform (PU) or non-uniform (PNU) qubit selection across different layers.

The numerical simulations show that AMA significantly outperforms the other three algorithms. Specifically, with the same number of optimization runs, AMA not only achieves the highest average approximation ratio, indicating superior stability but also drastically reduces the circuit depth and the number of quantum gates. The detailed resource comparison is as follows:

- On ER graphs, the AMA algorithm reduced circuit depth and the number of CNOT gates by 65.92% and 84.95%, respectively, compared with QAOA+. When compared with PU and PNU, AMA reduced circuit depth by 44.39% for both, and the number of CNOT gates by 77.21% and 77.01%.
- On 3-regular graphs, the AMA algorithm reduced circuit depth and the number of CNOT gates by 70.23% and 81.28%, respectively, compared with QAOA+. Compared with PU and PNU, AMA reduced circuit depth by 51.43% for both, and the number of CNOT gates by 68.69% for both.

The paper is organized as follows. Section II introduces the MIS problem and reviews the original QAOA and QAOA+ algorithms. Section III offers a detailed explanation of the AMA algorithm, including its key concepts and process. In Section IV, we present the performance comparison results of different algorithms. Finally, Section V summarizes the main contributions of this paper and discusses potential directions for future research.

## II. PRELIMINARIES

In this section, we review some relevant preliminaries to help readers better understand our work.

### A. The Maximum Independent Set Problem

Given an undirected graph  $G = (V, E)$ , where  $V = \{1, 2, \dots, n\}$  represents the set of vertices and  $E = \{\{u, v\} \mid u, v \in V, u \neq v\}$  denotes the set of edges. In graph theory, two vertices  $u$  and  $v$  are said to be \*adjacent\* if there exists an edge between them, i.e.,  $\{u, v\} \in E$ . A subset of vertices  $V_s \subseteq V$  is called an \*independent set\* if no two vertices in  $V_s$  are adjacent. In other words, for every pair of vertices  $u, v \in V_s$ , there is no edge between them, i.e.,  $\{u, v\} \notin E$ . A \*maximum independent set\* is an independent set that contains the

maximal number of vertices among all independent sets in the graph [40].

To formalize the MIS problem, a binary variable  $x_v$  for each vertex  $v \in V$  is introduced [14, 20], where  $x_v = 1$  if  $v$  belongs to the independent set  $V_s$ , and  $x_v = 0$  otherwise. A particular configuration of the vertices in the independent set can thus be represented by a bitstring  $x = x_1 x_2 \dots x_n$ , where each bit corresponds to whether a vertex is included in the independent set or not. There are  $2^n$  possible ways to assign values to the bits in  $x$ .

The objective of the MIS problem is to find a subset  $V_s$  that maximizes the number of vertices in the independent set, which is captured by the classical objective function

$$C(x) = \sum_{v=1}^n x_v, \quad (1)$$

subject to the independence constraint  $\sum_{(u,v) \in E} x_u x_v = 0$ , ensuring that no two vertices in  $V_s$  are adjacent. This constraint can be incorporated into the objective function using the Lagrange multiplier method, resulting in the following classical Hamiltonian [22]:

$$H_{\text{cla}}(x) = \sum_{v=1}^n x_v - \lambda \sum_{(u,v) \in E} x_u x_v, \quad (2)$$

where  $\lambda > 1$  is the Lagrange multiplier that enforces the independence constraint [27]. The first term in  $H_{\text{cla}}$  represents the objective to be maximized, while the second term penalizes the selection of adjacent vertices, ensuring that the solution respects the independence constraint. By maximizing this classical Hamiltonian, the optimal solution to the MIS problem can be found.

### B. Quantum Approximate Optimization Algorithm

In the QAOA framework, the MIS problem is encoded in the ground state (i.e., the minimal energy state) of a quantum target Hamiltonian  $H_C$ . This encoding is achieved by converting each binary variable  $x_v$  in  $-H_{\text{cla}}(x)$  to a quantum spin, which is represented by the operator  $\frac{I - \sigma_v^z}{2}$  [14], where  $\sigma_v^z$  denotes acting the Pauli-Z operator on the  $v$ -th qubit. The specific formulation of the quantum target Hamiltonian for the MIS problem in QAOA is given by

$$H_C = - \sum_{v=1}^n \left( \frac{I - \sigma_v^z}{2} \right) + \lambda \sum_{(u,v) \in E} \left( \frac{I - \sigma_u^z}{2} \right) \left( \frac{I - \sigma_v^z}{2} \right). \quad (3)$$

To achieve the MIS solution, QAOA starts with the ground state  $|s\rangle$  of the initial quantum Hamiltonian  $H_B$  and evolves toward the target ground state through a PQC constructed using a  $p$ -layer QAOA ansatz, where  $p$  is referred to as the layer depth, and the initial state  $|s\rangle$

is required to be easily implementable, meaning it can be prepared by a constant-depth (i.e., the circuit does not scale with the problem size) quantum circuit starting from the  $|0\rangle^{\otimes n}$  state.

Each layer of the QAOA ansatz consists of two unitary operators  $e^{-i\gamma_i H_C}$  and  $e^{-i\beta_i H_B}$ , where  $\gamma_i$  and  $\beta_i$  are the circuit parameters in the  $i$ -th layer of the QAOA ansatz, and  $i$  denotes the imaginary unit. In QAOA, the initial Hamiltonian is typically chosen as  $H_B = -\sum_{j=1}^n \sigma_j^x$  because its ground state  $|s\rangle = |+\rangle^{\otimes n}$  can be prepared using a depth-1 quantum circuit by applying a Hadamard gate to each qubit in the  $|0\rangle^{\otimes n}$  state, where  $\sigma_j^x$  represents acting the Pauli-X operator on the  $j$ -th qubit. The system evolves towards the ground state of the target Hamiltonian  $H_C$  through a PQC with the evolution controlled by the parameters  $\gamma_i$  and  $\beta_i$ .

The quantum state  $|s\rangle$  evolves through  $p$ -layer QAOA ansatz, resulting in the final quantum state

$$|\gamma_p, \beta_p\rangle = \prod_{i=1}^p e^{-i\beta_i H_B} e^{-i\gamma_i H_C} |s\rangle, \quad (4)$$

where  $\gamma_p = (\gamma_1, \gamma_2, \dots, \gamma_p)$  and  $\beta_p = (\beta_1, \beta_2, \dots, \beta_p)$  are the variational parameters in the PQC. The average expectation function value of the output state with respect to the target Hamiltonian is given by

$$F(\gamma_p, \beta_p) = \langle \gamma_p, \beta_p | H_C | \gamma_p, \beta_p \rangle. \quad (5)$$

The target ground state corresponds to the minimum expectation function value. Therefore, by minimizing this expectation function, QAOA can find the quantum state that encodes the optimal solution to the problem.

Multiple optimization runs are required to find the optimal parameters that minimize the expectation function. In each run, an initial set of parameters is assigned to the circuit, and the quantum state evolves according to the quantum circuit. The quantum computer then performs measurements to compute the expectation value of the target Hamiltonian. These results are passed to the classical optimizer, which updates the QAOA parameters  $(\gamma_p, \beta_p)$ . The updated parameters are sent back to the quantum computer for the next round of evolution and calculation. This process repeats until a stopping condition is met, such as convergence or reaching the maximum number of iterations [9, 20].

To quantify the quality of the final quantum state, the approximation ratio (AR)

$$r = \frac{F(\gamma_p, \beta_p)}{F_{\min}}, \quad (6)$$

is introduced [14, 20, 21], where  $F_{\min}$  is the ground state energy of  $H_C$ . The AR measures how close the output state provided by QAOA is to the ground state of  $H_C$ , with  $r \leq 1$ , where a value of 1 indicates the optimal solution.

### C. QAOA+

When solving the CCOPs using QAOA, the Hilbert space encompasses both feasible solutions and infeasible solutions. This leads to a large search space, and the algorithm may yield infeasible solutions upon termination. To address these limitations of QAOA, Hadfield et al. [30] proposed a novel quantum alternating operator ansatz algorithm, referred to as QAOA+. QAOA+ encodes the problem constraints into the initial Hamiltonian  $H_B$  and constructs a feasible space that only contains feasible solutions by alternatively applying  $p$ -layer QAOA+ ansatz on the initial quantum state  $|s\rangle$ , where  $|s\rangle$  is a feasible state that is easy to create [30]. By searching for the optimal solution within a feasible space, the size of the search space is reduced, and the probability of QAOA+ yielding invalid solutions is zero. Similar to the QAOA ansatz, each layer of the QAOA+ ansatz also consists of two unitary operators  $e^{-i\gamma_i H_C}$  and  $e^{-i\beta_i H_B}$ , but the specific implementation of the Hamiltonian in QAOA+ differs from QAOA. In the following, for the MIS problem, the designs of  $H_B$  and  $H_C$  in QAOA+ are introduced.

In QAOA+, the mixer unitary operator is required to preserve and explore the feasible solution space. Exploration refers to the evolution of the state from one feasible quantum state (i.e., a single feasible solution or a superposition of multiple feasible solutions) to another feasible state. Preservation ensures that no infeasible quantum states are generated during the evolution process. For the MIS problem, the quantum unitary operations acting on feasible states can be understood as analogous to classical operations, such as the removal or addition of vertices, on independent sets. To clarify this process, we analyze the conditions that must be satisfied when performing a classical operation on an independent set to generate a new independent set.

Denote the independent set as  $V'$ , and let the binary variable  $x_v = 1$  indicate that vertex  $v$  belongs to  $V'$  and  $x_v = 0$  otherwise. To add or remove vertices from  $V'$  without breaking its independence, the following conditions must be satisfied.

1. **Removing vertices from an independent set requires no additional conditions.** This is because removing vertices does not affect the independence of the remaining vertices and can result in another independent set. Successfully removing vertex  $v$  from  $V'$  corresponds to the state transition of  $x_v$  from 1 to 0.
2. **Adding a new vertex  $v_{\text{new}}$  to  $V'$  without destroying the independence constraint if and only if all its neighbors are not in  $V'$  (i.e., all neighboring vertices of  $v_{\text{new}}$  are in state 0).** Here,  $v_{\text{new}} \notin V'$  and  $v_{\text{new}} \in V$ . Successfully adding vertex  $v_{\text{new}}$  into  $V'$  corresponds to the state transition of  $x_{v_{\text{new}}}$  from 0 to 1.

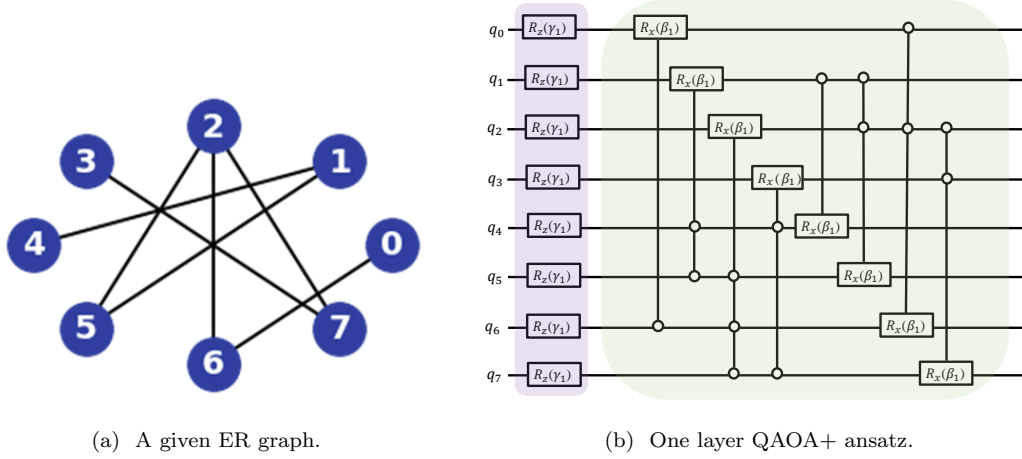


FIG. 1: The implementation of a single-layer QAOA+ ansatz for the given ER graph. (a) An ER graph with  $n = 8$  vertices. (b) The circuits with the green and purple undertone correspond to  $e^{-i\beta_1 H_B}$  and  $e^{-i\gamma_1 H_C}$ , respectively. Each qubit  $q_v$  corresponds to vertex  $v$ , where  $v = 0, 1, \dots, n-1$ .

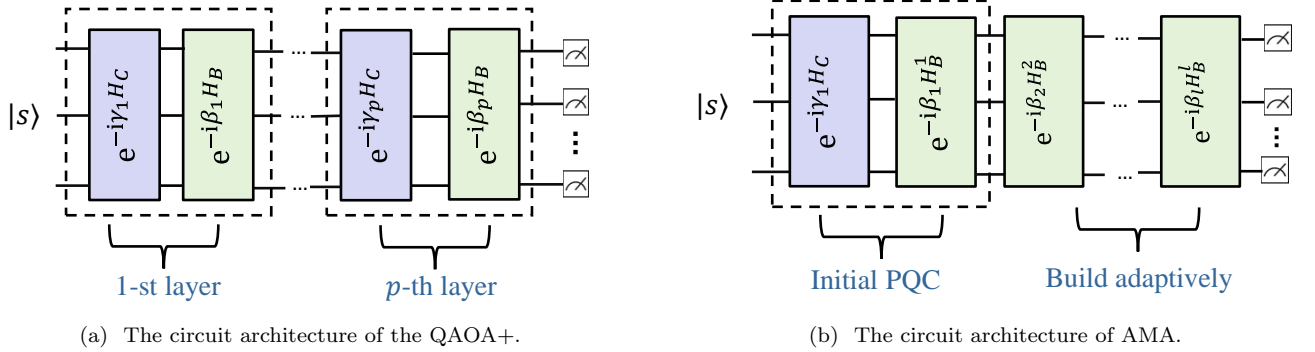


FIG. 2: The parameterized quantum circuit of QAOA+ and AMA, where  $H_C = -\sum_{v=1}^n \frac{I - \sigma_v^z}{2}$ . (a) In QAOA+, the PQC is built by  $p$ -layer QAOA+ ansatz, where one layer of QAOA+ ansatz has two unitary operations, and there are two optimized parameters in each layer. Notably, each qubit is acted on by the mixer when implementing each layer of the mixer unitary operator. (b) In the AMA algorithm, an initial PQC is first built by unitary operators  $U_C$  and  $U_M$ . In the subsequent layers, there is only one layer of mixer unitary operation  $e^{-i\beta_l H_B}$ . For  $l \geq 1$ , several mixers are randomly or adaptively added into  $e^{-i\beta_l H_B}$ .

All in all, without destroying the independence, the addition or removal of a vertex  $v$  can be controlled by the states of its neighbors. Specifically, the condition for adding or removing vertex  $v$  while maintaining the independence of the set is that all neighbors of  $v$  must not be in the independent set  $V'$ . This condition can be expressed as

$$f_v = \prod_{v_{q_j} \in N(v)} (1 - x_{v_{q_j}}) = 1, \quad (7)$$

where  $N(v)$  denotes the set of neighbors of vertex  $v$  that contains  $d(v)$  vertices, and  $x_{v_{q_j}}$  is the state of the  $q_j$ -th neighbor of  $v$ . The condition  $f_v = 1$  ensures that all neighbors of vertex  $v$  are not in the independent set  $V'$ , thus maintaining the independence of the set when  $v$  is

added or removed.

Successfully removing a vertex from  $V'$  or adding a vertex to  $V'$  corresponds to applying the  $X$  gate to the qubit corresponding to vertex  $v$ . If the operation fails (i.e., a vertex is not successfully removed or added), the identity operation  $I$  is applied instead. For each vertex  $v$ , its corresponding partial mixer Hamiltonian can be formally expressed as follows:

$$B_v = \sum_{f_v=1} |x_{v_{q_0}} x_{v_{q_1}} \dots x_{v_{q_d(v)}}\rangle \langle x_{v_{q_0}} x_{v_{q_1}} \dots x_{v_{q_d(v)}}| \otimes X_v + \sum_{f_v=0} |x_{v_{q_0}} x_{v_{q_1}} \dots x_{v_{q_d(v)}}\rangle \langle x_{v_{q_0}} x_{v_{q_1}} \dots x_{v_{q_d(v)}}| \otimes I_v. \quad (8)$$

In QAOA+, the total mixer Hamiltonian is given by  $H_B = \sum_{v=1}^n B_v$ , and the mixer unitary operator, pa-

parameterized by  $\beta_i$ , is expressed as

$$U_M(\beta_i) = e^{-i\beta_i H_B}. \quad (9)$$

For any vertex  $v$  with a degree greater than one, the implementation of  $e^{-i\beta_i H_B}$  corresponds to a multi-qubit controlled  $R_x$  gate, where the relevant qubits corresponding to the neighbors of  $v$  act as control qubits and the qubit corresponding to  $v$  serves as the target qubit. This implies that each vertex (represented by a qubit) has an associated multi-qubit controlled  $R_x$  gate. Since current quantum hardware is generally unable to directly implement multi-qubit controlled  $R_x$  gates, it is necessary to decompose them into a series of basic gates (e.g., controlled-NOT gates and rotation gates). As the number of control qubits increases, the resources and circuit depth required for this decomposition grow dramatically [38, 39], which limits the scale of optimization problems that can be handled by NISQ devices. Therefore, when solving the MIS problem using QAOA+, it is crucial to minimize not only the total number of multi-qubit controlled gates but also to prioritize reducing those with more control qubits. This is essential for solving larger-scale problems with limited resources in the NISQ era.

QAOA+ searches for the optimal solution within the feasible solution space, aiming to maximize the number of vertices in the independent set. The corresponding classical objective function is given in Eq. 1. To express this objective in the quantum domain, each  $x_v$  in the classical cost function  $-C(x)$  is replaced by the quantum operator  $(I - \sigma_v^z)/2$  [14], where  $\sigma_v^z$  represents acting the Pauli-Z operator on the  $v$ -th qubit. The quantum target Hamiltonian for the MIS problem in QAOA+ is given by

$$H_C = -\sum_{v=1}^n \frac{I - \sigma_v^z}{2}. \quad (10)$$

The corresponding target unitary operator for this Hamiltonian, parameterized by  $\gamma_i$ , is:

$$U_C(\gamma_i) = e^{-i\gamma_i H_C} = \prod_{v=1}^n R_z(\gamma_i, v), \quad (11)$$

which is composed of a sequence of single-qubit  $R_z$  rotation gates. These  $R_z(\gamma_i, v)$  gates apply a phase shift to the quantum state of qubit  $v$ , determined by the parameter  $\gamma_i$ . Importantly, while the  $R_z$  rotations modify the relative phase of the quantum state, they do not flip the individual qubits between the  $|0\rangle$  and  $|1\rangle$  states. As a result, the  $R_z$  operator only alters the amplitude (or phase) of the quantum state, rather than causing qubit-flip operations. For a better understanding of the PQC of the QAOA+, we give the implementation of a single-layer QAOA+ ansatz for a given ER graph in FIG. 1 and the circuit architecture of QAOA+ in FIG. 2a.

In summary, QAOA+ improves upon QAOA by encoding problem constraints into the initial Hamiltonian, re-

stricting the search to only feasible solutions. This effectively reduces unnecessary exploration, leading to a more efficient optimization process. However, in the QAOA+, mixers are applied to each qubit in each layer of the mixer unitary operator, which may result in high gate and circuit depth overheads. To reduce the number of mixers required by QAOA+ for solving CCOPs, the AMA algorithm is proposed. In the following, we will often refer to this multi-qubit controlled  $R_x$  operation as the ‘mixer’.

### III. THE ADAPTIVE MIXER ALLOCATION ALGORITHM

This section introduces the purpose and basic framework of the AMA algorithm.

AMA constructs a feasible solution space by applying the mixers to partial qubits in each layer of the mixer unitary operation, and then searches for the optimal solution within this space. Specifically, the AMA algorithm starts with an initial pre-trained PQC and incrementally adds a new layer of mixer unitary operation to the trained circuit. In each layer of the mixer unitary operation, only a subset of qubits is acted upon by the mixers, and these qubits are adaptively selected based on the evolution results of the trained circuit. After adding a new layer of mixer unitary operator, AMA optimizes all parameters in the entire circuit. In the subsequent steps, AMA repeats the process of adding the new layer of mixer unitary operation and performs parameter optimization for the whole circuit until a predefined stopping condition is satisfied, such as the expectation function reaches convergence.

Notably, the target unitary operator primarily influences the amplitude of the quantum state without directly affecting the flip of individual qubits. In contrast, the mixer unitary operator plays a more crucial role in each layer by influencing qubit flips, thereby facilitating the search process. To simplify computations and improve efficiency, we omit the target unitary operator in the subsequent layers, as done in Ref. [36], retaining only the mixer unitary operator.

All in all, AMA consists of three main steps, that is, constructing the initial pre-trained PQC, adaptively adding partial mixers for the new layer of mixer unitary operation, and optimizing the entire circuit. The circuit architecture of AMA is given in FIG. 2b, and an outline of the AMA pseudocode is shown in Algorithm 1. The details of constructing the initial PQC and selecting the mixers are as follows.

---

**Algorithm 1** Adaptive Mixer Allocation Algorithm
 

---

- 1: **Step 1:** Initialize the PQC  $U_{\text{init}}$  with a single layer of QAOA+ ansatz.
  - 2: **Step 2:** Initialize the operator pool  $U_{\text{pool}} = \{U(M_j) | j = 1, 2, \dots, n\}$ , and  $M_{\text{add}} = 0$ , where each mixer  $U(M_j)$  corresponds to an associated multi-qubit controlled  $R_x$  gate.
  - 3: **Step 3:** Adaptively select partial mixers from the operator pool  $U_{\text{pool}}$  and add them into the circuit  $U_{\text{init}}$ .
  - 4: **step 3.1** Compute the evaluation function value for each mixer in the current operator pool.
  - 5: **for**  $U(M_j)$  in  $U_{\text{pool}}$  **do**
  - 6:   Select the mixer  $U(M_j)$  from the operator pool  $U_{\text{pool}}$ .
  - 7:   Add the selected mixer  $U(M_j)$  to the circuit  $U_{\text{init}}$ , obtaining the current circuit  $U_{\text{cur}} = U_{\text{init}} + U(M_j)$ .
  - 8:   Generate multiple sets of parameters for the current circuit. Specifically, the parameters of the new layer of the mixer unitary are randomly generated, and the  $U_{\text{init}}$  reuses the optimized parameters.
  - 9:   Calculate the corresponding gradients (initial expectation function values) for the current circuit under different circuit parameters, then average the obtained gradients (initial expectation function values) to get  $F_{\text{gra}}$  ( $F_{\text{fun}}$ ).
  - 10:   Compute the corresponding evaluation function for the mixer  $U(M_j)$ .
  - 11: **end for**
  - 12: **step 3.2** Select one mixer that maximizes the evaluation function in the current operator pool  $U_{\text{pool}}$ , and this mixer is denoted as  $U(M_{j'}^*)$ .
  - 13: **step 3.3** Update the circuit  $U_{\text{init}} = U_{\text{init}} + U(M_{j'}^*)$  and the operator pool  $U_{\text{pool}} = U_{\text{pool}} - U(M_{j'}^*)$ ,  $M_{\text{add}} = M_{\text{add}} + 1$ .
  - 14: **while** the maximum  $F_{\text{gra}} > \delta_{\text{gra}}$  and  $M_{\text{add}} < \delta_{\text{add}}$  **do**
  - 15:   Repeat **step 3.1 -step 3.3**.
  - 16: **end while**
  - 17: **Step 4:** Optimize the entire circuit  $U_{\text{init}}$ , where AMA randomly generates the parameters of the newly added mixer unitary operation and reuses the parameters of the optimized circuit.
  - 18: **while** stopping condition not met **do**
  - 19:   Repeat **Step 2 - Step 4** until reaching the pre-defined stop condition.
  - 20: **end while**
- 

**A. The construction of the initial pre-trained PQC**

In the AMA algorithm, the initial pre-trained PQC is first constructed using a single layer of the QAOA+ ansatz. During the implementation of the mixer unitary operation  $e^{-i\beta_1 H_B}$ , to reduce the number of mixers, only a subset of qubits is randomly selected for applying the mixers. Given that the implementation cost of

single-qubit rotation gates  $R_z$  is relatively low, these  $R_z$  gates are applied to all qubits when constructing the target unitary operator. Once the initial circuit is built, its parameters are randomly initialized. The parameters are subsequently optimized using a classical optimizer, yielding the optimized PQC, denoted as  $U_{\text{init}}$ .

**B. Adaptively selecting the mixers**

Since each qubit is associated with a unique multi-qubit controlled  $R_x$  gate (mixer), selecting which qubits to apply the mixers to is equivalent to selecting which mixers from the operator pool  $U_{\text{pool}} = \{U(M_j) | j = 1, 2, \dots, n\}$  to add into the new layer of the mixer unitary operator. In this work, an evaluation function is used to guide the selection of mixers from the pool for each layer. Specifically, the evaluation function is defined as

$$C = (1 - f_1) * F_{\text{fun}} + f_1 * F_{\text{gra}}, \quad (12)$$

where  $f_1$  is a coefficient between 0 and 1,  $F_{\text{fun}}$  and  $F_{\text{gra}}$  represent the average initial expectation function value and the average gradient, respectively. During the mixer selection process,  $F_{\text{fun}}$  and  $F_{\text{gra}}$  are calculated by averaging the initial expectation function values and gradients across multiple sets of randomly chosen parameters. First, several sets of random initial parameters are generated, and the corresponding gradient values and initial expectation function values for the circuit under these parameter sets are computed. Then,  $F_{\text{gra}}$  and  $F_{\text{fun}}$  are obtained by averaging the gradients and the initial expectation function values, respectively.

The design of the evaluation function provides two main advantages in the selection process. First, by averaging gradients and expectation values, it reduces the influence of randomness that could arise from using a single set of initial parameters. Second, it takes into account both the optimization direction (via the gradient) and the quality of the solution (via the expectation function), which may lead to better results compared with methods relying on only one factor.

AMA sequentially selects the mixer that maximizes the evaluation function from the operator pool and adds it to the circuit. Specifically, for each mixer in  $U_{\text{pool}}$ , AMA computes its corresponding evaluation function value, selects the mixer  $U(M_{j'}^*)$  that maximizes the evaluation function from the operator pool  $U_{\text{pool}} = \{U(M_j) | j = 1, 2, \dots, n\}$ . The selected mixer is added to the pre-trained circuit  $U_{\text{init}}$ , resulting in a new circuit  $U_{\text{init}} = U_{\text{init}} + U(M_{j'}^*)$ . Then, the operator pool is updated by removing the selected mixer, updating  $U_{\text{pool}} = U_{\text{pool}} - U(M_{j'}^*)$ . The process of selecting the mixer, adding it to the circuit, and updating the operator pool is repeated until the stopping condition is met, such as the number of added mixers  $M_{\text{add}}$  reaching the upper limit  $\delta_{\text{add}}$ , or the maximal  $F_{\text{gra}}$  falling below

the threshold  $\delta_{\text{grad}}$ . In this way, AMA adaptively constructs the new layer of mixer unitary operations. Notably, considering the impact of different mixer arrangements on the circuit's optimization, AMA selects mixers sequentially based on the evaluation function, rather than adding multiple mixers at once in a random order. This approach may ensure that the mixers are added in a systematic manner, leading to more effective circuit optimization.

#### IV. NUMERICAL SIMULATIONS

We randomly generated graphs with  $n = 8, 10, 12$ , with each size comprising 20 ER graphs and 20 3-regular graphs. On these given graphs, we evaluated the performance of the AMA algorithm. Furthermore, we compared its performance with QAOA+, PU, and PNU, where PU and PNU are intuitive ways to apply mixers to partial qubits. In the numerical simulation experiments, the initial state of the circuit for all four algorithms was set to  $|0\rangle^{\otimes n}$ , and the optimization round or run is stopped when the expectation function reaches convergence. For the AMA algorithm, we set  $f_1 = 0.5$ , and the termination condition in each run was defined as the change in the obtained expected value being less than 0.1 in two consecutive parameter optimizations. For QAOA+, PU, and PNU, the layer depth was set to  $p = 4, 5, 6$ , and each algorithm was executed for 100 optimization runs at each layer depth. For PU and PNU, the number of mixers in each layer was set to  $N_{\text{pm}} = \lfloor n/2 \rfloor + 1$  for different graph sizes  $n$ , and the partial qubits acted on by mixers were randomly selected.

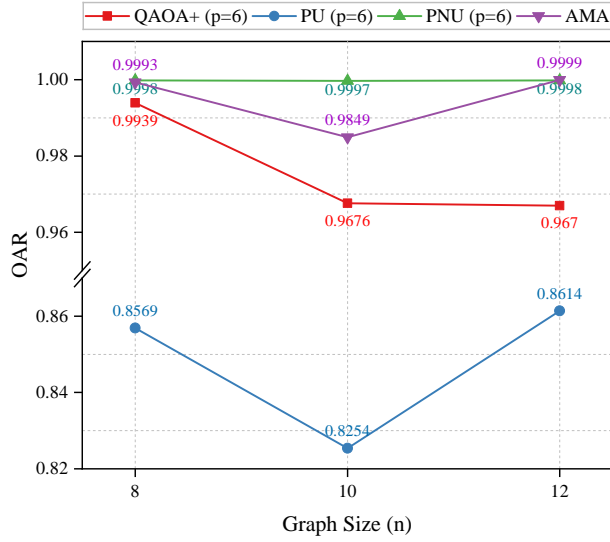
To compare the performance of these four algorithms under the same number of optimization runs, the experiments measured the optimal approximation ratio (OAR), average approximation ratio (AAR), total number of iterations (ITRs), total quantum runtime, total circuit depths (CDs), and total CNOT gates (CNOTs) required for implementing the mixers. Here, we estimate the runtime based on the calculation method provided in Ref. [20, 41], and the circuit depth was approximated by calling the DAGCircuit interface in Mindspore Quantum [42]. It is important to note that MindSpore Quantum does not decompose each multi-qubit controlled  $R_x$  gate into basic gates for the purpose of circuit depth calculation. Instead, it directly estimates the circuit depth of the quantum circuit containing multi-qubit controlled gates. However, for the calculation of the number of CNOT gates, we first decompose the multi-qubit controlled gates into basic gates, as outlined in Ref. [39], and then compute the corresponding number of CNOT gates.

The numerical simulation results show that as the layer depth  $p$  increases, the OARs obtained by QAOA+, PU, and PNU gradually improve and approach the OAR achieved by the AMA algorithm. In the main text, we

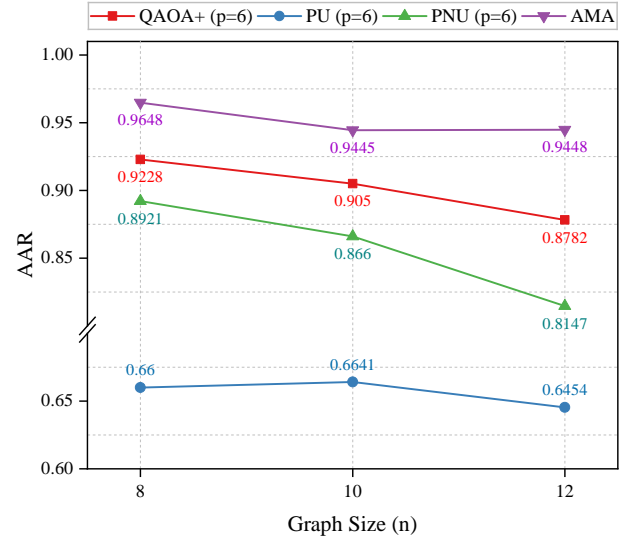
compare the results of the three algorithms with  $p = 6$  to those of the AMA algorithm, and more details are shown in FIG. 3 and FIG. 4. The corresponding data with  $p = 4, 5$  are presented in the Appendix A1. In the following, we mainly take the performance of the algorithms on ER graphs as an example to carry out the relevant numerical analysis.

We plot the OAR and AAR obtained by different algorithms on the given graphs. The OAR is defined as the maximum approximation ratio obtained in multiple optimization runs, and it reflects the best performance of the algorithm across all optimization runs, providing a measure of the highest-quality solution achieved during the experiments. The AAR is the average of the approximation ratios obtained in multiple optimization runs, and it reflects the average performance across all runs, providing a measure of stability and consistency. From the numerical results shown in FIG. 3a and FIG. 3b, it can be observed that compared with the QAOA+ and PNU algorithms, the ARs obtained by the PU algorithm are the lowest under the same layer depth and the same number of optimization runs, which is because the search space constructed by the PU algorithm is limited, and this space may not include the high-quality solution especially when some qubits in the MIS solution are not acted on by the mixers. In contrast, the PNU algorithm mitigates this issue by randomly adjusting the diversity of qubits that are acted on by mixers in each layer of the mixer unitary operator, allowing more and various qubits to participate in the exploration of the feasible solution space. This approach reduces the likelihood of missing critical qubits and compensates for the deficiencies of the PU algorithm. Numerical results in FIG. 3 and FIG. 4 both show that under the same number of optimization runs, compared with QAOA+, PNU can achieve higher-quality solutions with fewer mixers. Similarly, compared with PU, PNU can achieve higher-quality approximate solutions using the same number of mixers. However, determining the number of mixers required in each layer of the mixer unitary and selecting the qubits that are acted on by mixers remain challenging tasks for the PNU algorithm. If the number is set too small, the expressivity of the PQC may be insufficient. If it is set too large, it may include redundant mixers, leading to wasted quantum resources.

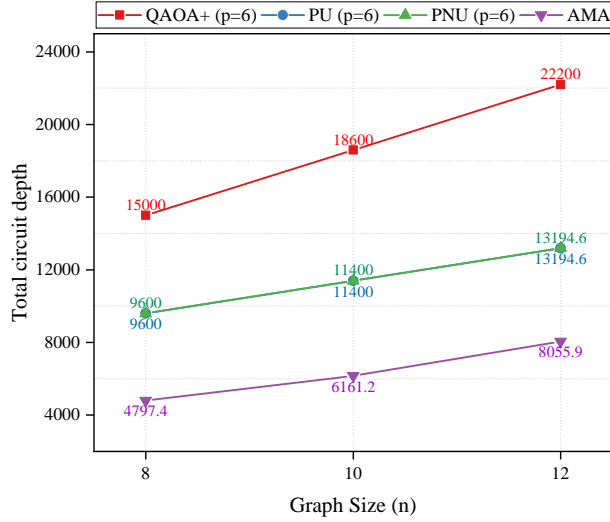
The AMA algorithm dynamically adjusts the mixers for the next layer of mixer unitary based on the evolution results of the optimized circuit, thus flexibly setting the number of mixers required in each layer. **FIG. 3a and FIG. 3b show that compared with the other three algorithms, the AMA algorithm achieves both a higher OAR and the largest AAR under the same number of optimization runs. This indicates that AMA exhibits better stability and robustness. In addition, FIG. 3c and FIG. 3d show that the AMA algorithm significantly reduces the circuit depth and the number of CNOT gates re-**



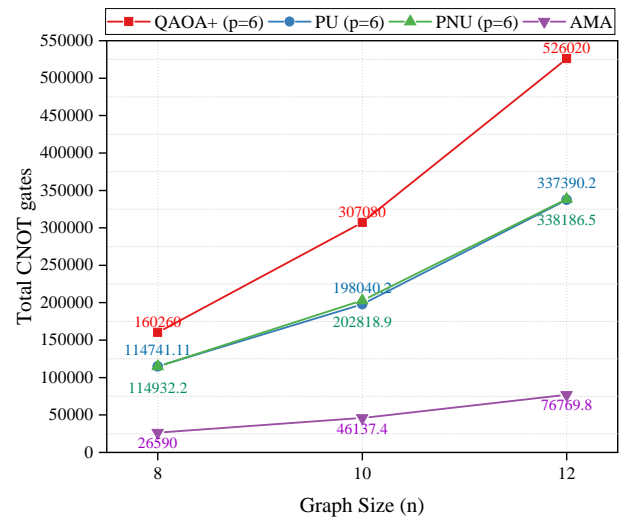
(a) The obtained OAR.



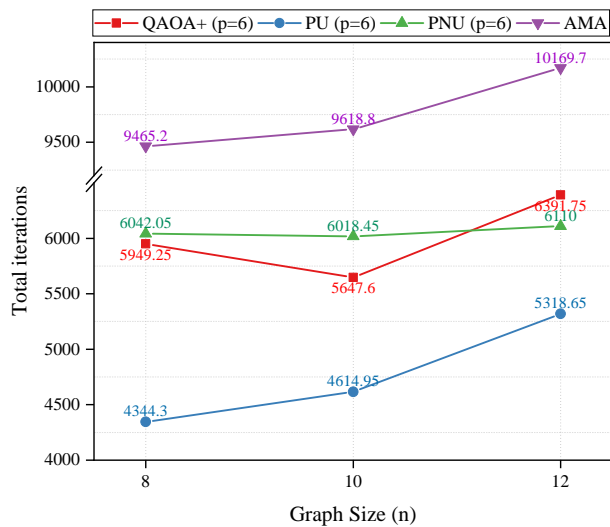
(b) The obtained AAR.



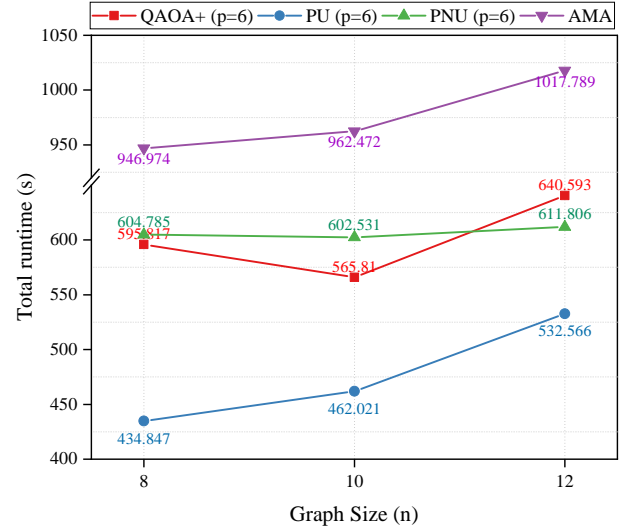
(c) The total circuit depth.



(d) The total CNOT gates.



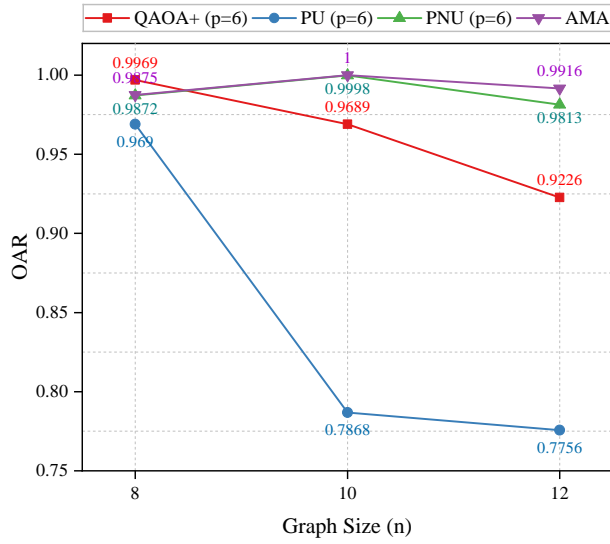
(e) The total iterations.



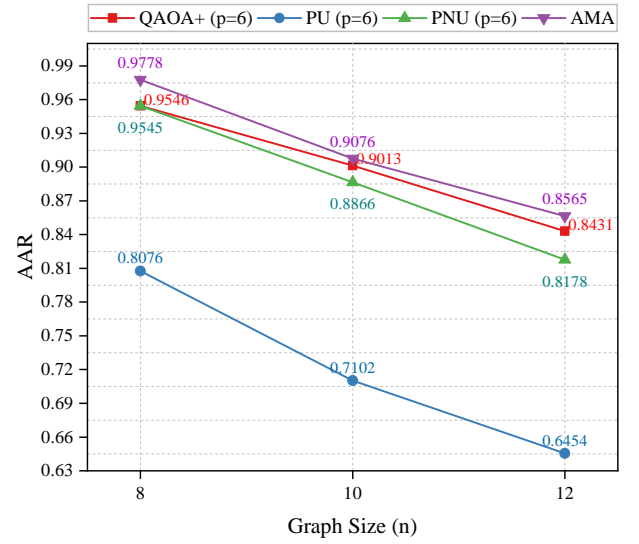
(f) The total runtime.

FIG. 3: The performance of different algorithms on ER graphs with various graph size.

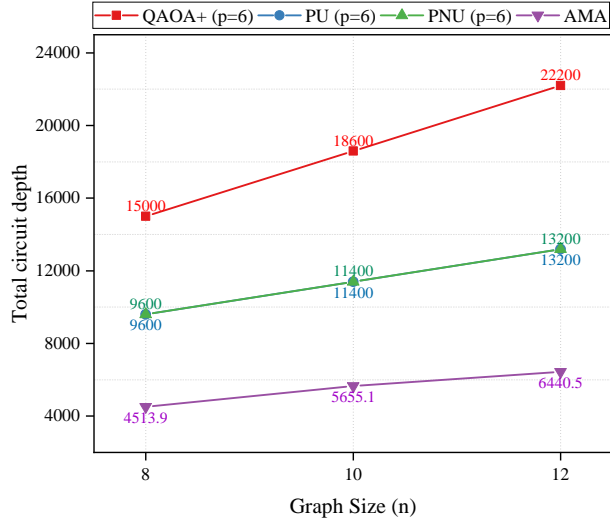




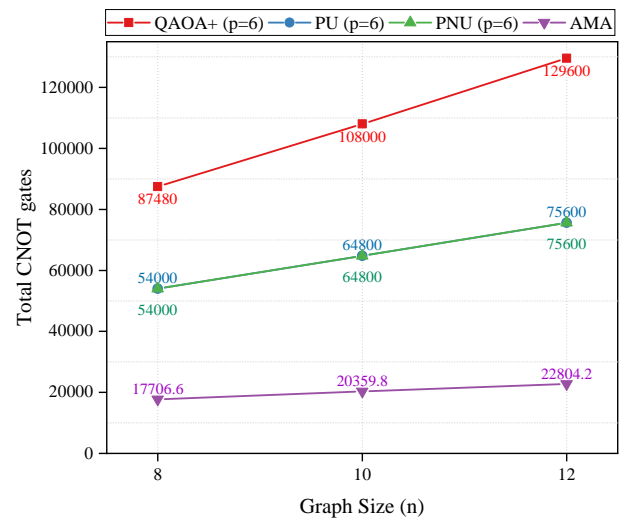
(a) The obtained OAR.



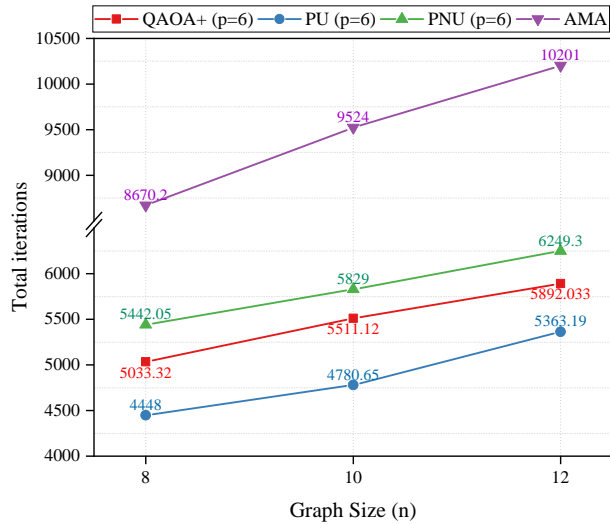
(b) The obtained AAR.



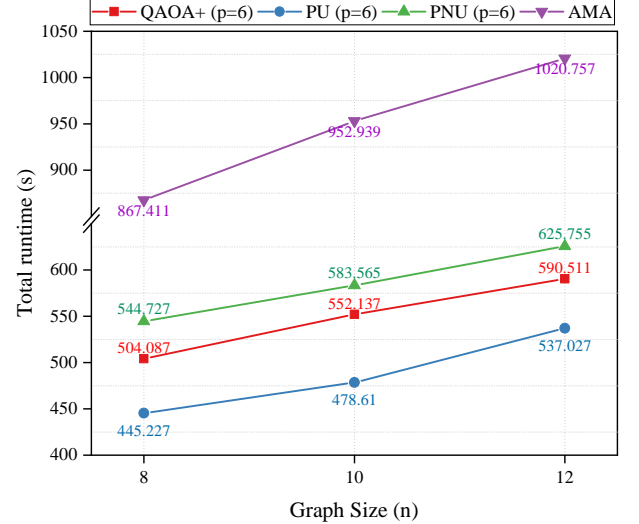
(c) The total circuit depth.



(d) The total CNOT gates.



(e) The total iterations.



(f) The total runtime.

FIG. 4: The performance of different algorithms on 3-regular graphs with various graph size.

**quired to implement the PQC.** This resource optimization may mitigate noise accumulation in quantum circuits, enhancing both solution stability and quality. The detailed consumption is as follows.

- On ER graphs, the AMA algorithm reduced circuit depth and the number of CNOT gates by 65.92% and 84.95%, respectively, compared with QAOA+. When compared with PU and PNU, AMA reduced circuit depth by 44.39% for both, and the number of CNOT gates by 77.21% and 77.01%.
- On 3-regular graphs, the AMA algorithm reduced circuit depth and the number of CNOT gates by 70.23% and 81.28%, respectively, compared with QAOA+. Compared with PU and PNU, AMA reduced circuit depth by 51.43% for both, and the number of CNOT gates by 68.69% for both.

**All in all, these results demonstrate that AMA significantly reduces the required number of CNOT gates and circuit depth per iteration while maintaining high solution quality.**

The simulation results in FIG. 3e and FIG. 3f suggest that the total number of iterations and runtime consumed by the AMA algorithm is more than the other three algorithms under the same number of optimization runs. This is because AMA involves multiple rounds of parameter optimization per run, which increases the number of iterations and, consequently, the quantum runtime. Although the number of iterations is important, the circuit depth and gate resource requirements in a single run more directly determine the problem sizes that hardware can support on resource-constrained quantum devices. Excessively high gate and depth demands in each iteration may prevent the hardware from solving larger-scale problems. In this paper, **the AMA algorithm trades off a portion of the iteration count to optimize the gate and circuit depth resources required per iteration, enabling current devices to solve larger-scale problems within fixed hardware limitations.**

Overall, the analysis of simulation results highlights the superiority of the AMA algorithm over QAOA+, PU, and PNU in both performance and resource savings. The AMA algorithm reduces gate and circuit depth resources in each run. Under this resource trade-off, it not only improves solution quality and stability but also significantly expands the applicability of current devices. The AMA algorithm may provide a practical optimization pathway for resource-constrained NISQ devices to tackle more complex problems and lay the foundation for addressing larger-scale quantum computing tasks in the future. In addition to comparing the solution quality and resource consumption under the same number of runs, we also provide in the Appendix A 2 the quantum resources

consumed by each algorithm to achieve the same near-optimal solution, which is to more intuitively reflect the efficiency of each algorithm.

## V. CONCLUSION AND OUTLOOK

To mitigate the gate and circuit depth overheads when using QAOA+ to solve CCOPs, we introduced the AMA algorithm. AMA constructs a feasible space by adaptively applying partial mixers in each layer of the mixer unitary operator, and then searches for the optimal solution within this constrained space. The performance of the AMA algorithm was evaluated on the MIS problem and compared with the original QAOA+, PU, and PNU algorithms. Numerical results showed that, for the same number of optimization runs, AMA achieved superior performance. Specifically, AMA obtained higher OARs and AARs (indicating higher solution quality and greater stability), along with significantly reduced resource consumption, including reductions in circuit depth and CNOT gates compared with QAOA+ variants. These results highlight the feasibility and efficiency of the AMA algorithm. The adaptive nature of AMA, which reduces quantum resource demands while maintaining solution quality, makes it a crucial tool for overcoming the limitations of current quantum hardware, particularly for resource-constrained NISQ devices.

Although the current work only demonstrates the efficiency of the AMA algorithm in solving the MIS problem, AMA is a general algorithm that is not limited to MIS and can be applied to solving a variety of CCOPs. Further research is needed to explore its application to other CCOPs and evaluate its scalability and robustness for larger problem sizes and different graph types. This will help extend its applicability and increase its utility for diverse optimization tasks. Future work could also focus on refining the optimization and initialization strategies for AMA. For instance, incorporating deep learning techniques could improve the prediction of better initial parameters, accelerating convergence and enhancing optimization efficiency. Additionally, evaluating its performance on real quantum hardware is essential to understand its behavior in noisy environments and assess its practical advantages and challenges.

The AMA algorithm represents a significant advancement in leveraging quantum computing to solve CCOPs, and its further development may have a profound impact on addressing real-world optimization challenges with quantum advantage.

## VI. ACKNOWLEDGEMENTS

Thanks for the support provided by Mindspore Community. Thanks for the valuable suggestions from Ziwen Huang. This work is supported by National Natural Science Foundation of China (Grant Nos. 62371069, 62372048, 62272056 ), and BUPT Excellent Ph.D. Students Foundation(CX2023123).

- 
- [1] L. K. Grover, in *Proceedings of the Twenty-Eighth Annual ACM Symposium on Theory of Computing*, STOC '96 (Association for Computing Machinery, New York, NY, USA, 1996) p. 212–219.
- [2] P. Shor, in *Proceedings 35th Annual Symposium on Foundations of Computer Science* (IEEE, 1994) pp. 124–134.
- [3] A. W. Harrow, A. Hassidim, and S. Lloyd, *Phys. Rev. Lett.* **103**, 150502 (2009).
- [4] J. Preskill, *Quantum* **2**, 79 (2018).
- [5] A. Peruzzo, J. McClean, P. Shadbolt, M.-H. Yung, X.-Q. Zhou, P. J. Love, A. Aspuru-Guzik, and J. L. O’Brien, *Nature Communications* **5** (2014), 10.1038/ncomms5213.
- [6] H. R. Grimsley, S. E. Economou, E. Barnes, and N. J. Mayhall, *Nature Communications* **10** (2019), 10.1038/s41467-019-10988-2.
- [7] H. L. Tang, V. Shkolnikov, G. S. Barron, H. R. Grimsley, N. J. Mayhall, E. Barnes, and S. E. Economou, *PRX Quantum* **2**, 020310 (2021).
- [8] R. LaRose, A. Tikku, E. O’Neel-Judy, L. Cincio, and P. Coles, *npj Quantum Information* **5**, 8 (2019).
- [9] H.-L. Liu, Y.-S. Wu, L.-C. Wan, S.-J. Qin, S.-J. Qin, F. Gao, and Q.-Y. Wen, *Phys. Rev. A* **104**, 022418 (2021).
- [10] Y. Du, T. Huang, S. You, M.-H. Hsieh, and D. Tao, *npj Quantum Information* **8**, 62 (2022).
- [11] Q. Xiong, Y. Fei, Q. Du, B. Zhao, S. Di, and Z. Shan, *Quantum Science and Technology* **10**, 015007 (2024).
- [12] Y. Song, Y. Wu, S. Wu, D. Li, Q. Wen, S. Qin, and F. Gao, *Science China Physics, Mechanics & Astronomy* **67**, 250311 (2024).
- [13] L. Li, J. Li, Y. Song, S. Qin, Q. Wen, and F. Gao, *Science China Physics, Mechanics & Astronomy* **68**, 1 (2025).
- [14] E. Farhi, J. Goldstone, and S. Gutmann, “A quantum approximate optimization algorithm,” (2014), arXiv:1411.4028 [quant-ph].
- [15] S. Bravyi, A. Kliesch, R. Koenig, and E. Tang, *Phys. Rev. Lett.* **125**, 260505 (2020).
- [16] L. Zhu, H. L. Tang, G. S. Barron, F. A. Calderon-Vargas, N. J. Mayhall, E. Barnes, and S. E. Economou, *Phys. Rev. Res.* **4**, 033029 (2022).
- [17] Z. Wang, N. C. Rubin, J. M. Dominy, and E. G. Rieffel, *Phys. Rev. A* **101**, 012320 (2020).
- [18] L. Zhou, S.-T. Wang, S. Choi, H. Pichler, and M. D. Lukin, *Phys. Rev. X* **10**, 021067 (2020).
- [19] J. Wurtz and D. Lykov, *Phys. Rev. A* **104**, 052419 (2021).
- [20] X.-H. Ni, B.-B. Cai, H.-L. Liu, S.-J. Qin, F. Gao, and Q.-Y. Wen, *Advanced Quantum Technologies* **7**, 2300419 (2024).
- [21] S. H. Sack and M. Serbyn, *Quantum* **5**, 491 (2021).
- [22] J. R. Finžgar, A. Kerschbaumer, M. J. Schuetz, C. B. Mendl, and H. G. Katzgraber, *PRX Quantum* **5**, 020327 (2024).
- [23] L. T. Brady and S. Hadfield, *Phys. Rev. A* **110**, 052435 (2024).
- [24] P. Vikstål, M. Grönkvist, M. Svensson, M. Andersson, G. Johansson, and G. Ferrini, *Phys. Rev. Appl.* **14**, 034009 (2020).
- [25] A. Bengtsson, P. Vikstål, C. Warren, M. Svensson, X. Gu, A. F. Kockum, P. Krantz, C. Križan, D. Shiri, I.-M. Svensson, G. Tancredi, G. Johansson, P. Delsing, G. Ferrini, and J. Bylander, *Phys. Rev. Appl.* **14**, 034010 (2020).
- [26] Y. Zhang, X. Mu, X. Liu, X. Wang, X. Zhang, K. Li, T. Wu, D. Zhao, and C. Dong, *Applied Soft Computing* **118**, 108554 (2022).
- [27] A. Lucas, *Frontiers in Physics* **2** (2014), 10.3389/fphy.2014.00005.
- [28] C. Papalitsas, T. Andronikos, K. Giannakis, G. Theocharopoulou, and S. Fanarioti, *Algorithms* **12** (2019), 10.3390/a12110224.
- [29] Y. Ruan, Z. Yuan, X. Xue, and Z. Liu, *Information Sciences* **619**, 98 (2023).
- [30] S. Hadfield, Z. Wang, B. O’gorman, E. G. Rieffel, D. Venturelli, and R. Biswas, *Algorithms* **12**, 34 (2019).
- [31] S.-S. Wang, H.-L. Liu, Y.-Q. Song, F. Gao, S.-J. Qin, and Q.-Y. Wen, *Physica A: Statistical Mechanics and its Applications* **626**, 129089 (2023).
- [32] N. Xie, X. Lee, D. Cai, Y. Saito, N. Asai, and H. C. Lau, *Quantum Information Processing* **23**, 291 (2024).
- [33] T. Tomesh, Z. H. Saleem, and M. Suchara, *Quantum* **6**, 781 (2022).
- [34] X.-H. Ni, L.-X. Li, Y.-Q. Song, Z.-P. Jin, S.-J. Qin, and F. Gao, “Progressive quantum algorithm for maximum independent set with quantum alternating operator ansatz,” (2024), arXiv:2405.04303 [quant-ph].
- [35] S. Hadfield, T. Hogg, and E. G. Rieffel, *Quantum Science and Technology* **8**, 015017 (2022).
- [36] S.-S. Wang, H.-L. Liu, Y.-M. Li, F. Gao, S.-J. Qin, and Q.-Y. Wen, *Advanced Quantum Technologies* **n/a**, 2400201.
- [37] M. Fingerhuth, T. Babej, and C. Ing, “A quantum alternating operator ansatz with hard and soft constraints for lattice protein folding,” (2018), arXiv:1810.13411 [quant-ph].
- [38] R. Vale, T. M. D. Azevedo, I. C. S. Araújo, I. F. Araujo, and A. J. da Silva, *IEEE Transactions on Computer-Aided Design of Integrated Circuits and Systems* **43**, 802 (2024).
- [39] T. Tomesh, N. Allen, D. Dilley, and Z. Saleem, *Quantum* **8**, 1493 (2024).
- [40] J. Robson, *Journal of Algorithms* **7**, 425 (1986).
- [41] G. G. Guerreschi and A. Y. Matsuura, *Scientific reports* **9**, 6903 (2019).
- [42] X. Xu, J. Cui, Z. Cui, R. He, Q. Li, X. Li, Y. Lin, J. Liu, W. Liu, J. Lu, M. Luo, C. Lyu, S. Pan, M. Pavel, R. Shu, J. Tang, R. Xu, S. Xu, K. Yang, F. Yu, Q. Zeng, H. Zhao, Q. Zheng, J. Zhou, X. Zhou, Y. Zhu, Z. Zou, A. Bayat, X. Cao, W. Cui, Z. Li, G. Long, Z. Su, X. Wang, Z. Wang, S. Wei, R.-B. Wu, P. Zhang, and M.-H. Yung, “Mind-spore quantum: A user-friendly, high-performance, and ai-compatible quantum computing framework,” (2024), arXiv:2406.17248 [quant-ph].

## Appendix A: The performance comparison among different algorithms

### 1. The obtained AR and total resource consumption of various algorithms under $p = 4, 5$

The choice of depth  $p$  can affect the performance of the QAOA+, PNU, and PU algorithms, which in turn influences how they compare with the AMA algorithm. The main text compares the results of QAOA+, PNU, and PU with AMA at  $p = 6$ . This subsection presents additional comparisons at  $p = 4$  and  $p = 5$ , focusing on the performance metrics of each algorithm. The comparisons include the approximation ratios, as well as resource consumption metrics—such as iterations, circuit depth, CNOT gates, and runtime—across multiple runs for each algorithm at different depths.

The numerical results in Tables A1 and A2 demonstrate that, under the same number of runs, the AMA algorithm not only achieves a higher OAR (i.e., higher quality solutions) but also exhibits a significantly higher AAR than the other algorithms (i.e., more stable performance). Moreover, the simulation results show that the circuit depth and the number of CNOT gates consumed by AMA are considerably lower than those of the other algorithms, highlighting its advantage in reducing gate resource usage and circuit depth. However, due to the multi-round optimization process involved in each run of AMA, its iteration count is higher than that of the other algorithms. This increased iteration count directly affects the runtime, resulting in AMA consuming the most runtime for the same number of runs. The additional numerical results presented here are consistent with the conclusions drawn in the main text.

By providing the additional data, the goal is to ensure that the experimental comparison remains fair and unbiased with respect to layer depth selection, thereby enhancing the accuracy and comprehensiveness of the algorithm performance comparison. Specifically, in the numerical simulation experiments, we did not deliberately choose larger layer depths to artificially increase the gate resources and circuit depth required by the compared algorithms in order to highlight the advantage of AMA in saving resources. Similarly, we did not select deliberately shallow layer depths to reduce the approximation ratio of the compared algorithms, thus ensuring that AMA's ability to achieve high-quality solutions is accurately represented.

### 2. The total resources consumed by various algorithms when they achieve the given OAR.

In the previous section, we compared the optimal solutions and resource consumption of different algorithms under the same number of runs. However, comparing based solely on the same number of runs has its limi-

tations, as some algorithms may achieve the same OAR with fewer runs. If we only compare based on a fixed number of runs, it may lead to an underestimation of the efficiency of more efficient algorithms. To provide a more balanced evaluation of algorithm performance, we further compare the resource consumption of each algorithm when achieving the same given OAR, offering a more direct reflection of the actual efficiency of each algorithm.

Due to the poor performance of the PU algorithm, which fails to provide competitive results in comparison to the other algorithms, we focus here on comparing the performance of PNU, QAOA+, and AMA. To calculate the resource consumption of QAOA+ and PNU at a given OAR, we set different layer depths from 1 to  $n$ , and conducted  $200p$  optimization runs at each layer depth. For each layer depth, we computed the average circuit depth, CNOT gates, runtime, and iterations per run, and also calculated the OAR obtained in multiple runs at each layer depth. We then determined the minimum layer depth required for each algorithm to achieve the given OAR and computed the number of times the algorithm reached the given OAR at this minimum layer depth (denoted as  $s$ ). We regarded the ratio of  $s$  to the total runs  $c$  at that depth as the probability of the algorithm achieving the OAR, and its reciprocal as the expected number of runs required to achieve the OAR, denoted as  $T_{\text{avg}}$ . Furthermore, the product of  $T_{\text{avg}}$  and the average circuit depth (CNOT, runtime, iterations) per run at the minimum layer depth gives the estimated average total circuit depth (CNOT, runtime, iterations) required for the algorithm to reach the given OAR. For the AMA algorithm, we performed  $50n$  optimization runs for each graph and computed the average total number of runs for AMA to reach the given OAR, as well as the average resource consumption per run. Additionally, we computed the average total resource consumption for the AMA algorithm when reaching the given OAR. For each graph, we performed the calculations as described above and took the average across multiple graph instances to represent the average total resource consumption of the algorithm across different graph types. FIG. A1 and A2 show the actual average total consumption of the QAOA+, PNU, and PU algorithms when reaching the given OAR on ER and 3-regular graphs.

The numerical simulation results show that the total resource consumption required for the algorithms to achieve a given OAR increases as the OAR requirement rises. When the OAR requirement is low, the QAOA+ algorithm consumes slightly more resources than AMA and fewer resources than PNU. However, as the OAR requirement increases, the resource consumption of QAOA+ quickly exceeds that of PNU and AMA, showing a significant gap in resource demand. For ER (3-regular) graphs of the same size, the AMA algorithm generally achieves the given OAR with fewer resources, and this advantage becomes more pronounced as the OAR increases. This

TABLE A1: The obtained AR and total resource consumption by different algorithms under the same number of runs on ER graphs.

Algo.	$p$	$n$	OAR	AAR	total-ITRs	total-CDs	total-CNOTs	total-runtime
AMA	-	8	0.9993	0.9648	9465.2	4797.4	26590.0	946.974
	-	10	0.9849	0.9445	9618.8	6161.2	46137.4	962.472
	-	12	0.9999	0.9488	10169.7	8055.9	76769.8	1017.789
QAOA+	4	8	0.9538	0.8871	5143.2	10000.0	106840.0	514.834
	4	10	0.9448	0.8827	5001.2	12400.0	204720.0	500.740
	4	12	0.9111	0.8409	5327.1	14800.0	350680.0	533.498
	5	8	0.9819	0.9107	5652.4	12500.0	133550.0	565.946
	5	10	0.9584	0.9010	5498.1	15500.0	255900.0	550.662
	5	12	0.9461	0.8651	5998.9	18500.0	438350.0	600.990
PU	4	8	0.8486	0.6577	4495.9	6400.0	76283.2	449.877
	4	10	0.8277	0.6484	4570.5	7600.0	133760.0	457.397
	4	12	0.8532	0.6282	4968.5	8800.0	225873.6	497.287
	5	8	0.8558	0.6639	4470.3	8000.0	96119.5	447.382
	5	10	0.8251	0.6616	4738.0	9500.0	166048.0	474.250
	5	12	0.8599	0.6395	5152.7	11000.0	282431.0	515.837
PNU	4	8	0.9993	0.8106	5147.0	6400.0	76629.2	515.029
	4	10	0.9893	0.8052	5203.3	7600.0	135471.2	520.725
	4	12	0.98	0.7459	5268.7	8800.0	225087.4	527.334
	5	8	0.9998	0.8586	5766.4	8000.0	95985.8	577.101
	5	10	0.9863	0.8430	5644.3	9500.0	169550.6	564.966
	5	12	0.9965	0.7838	5776.5	11000.0	282052.4	578.285

TABLE A2: The obtained AR and total resource consumption by different algorithms under the same number of runs on 3-regular graphs.

Algo.	$p$	$n$	OAR	AAR	total-ITRs	total-CDs	total-CNOTs	total-runtime
AMA	-	8	0.9875	0.9778	8670.2	4513.9	17706.6	867.411
	-	10	0.9999	0.9076	9524.0	5655.1	20359.8	952.939
	-	12	0.9916	0.8565	10201.0	6440.5	22804.2	1020.757
QAOA+	4	8	0.9889	0.9451	4598.3	10000.0	58320.0	460.290
	4	10	0.9343	0.8877	4854.2	12400.0	72000.0	486.022
	4	12	0.8738	0.8278	5181.8	14800.0	86400.0	518.947
	5	8	0.9943	0.9522	4930.3	12500.0	72900.0	493.646
	5	10	0.9534	0.8954	5315.8	15500.0	90000.0	532.404
	5	12	0.8990	0.8371	5615.3	18500.0	108000.0	562.569
PU	4	8	0.9658	0.7847	4396.6	6400.0	36000.0	439.941
	4	10	0.7870	0.7047	4490.4	7600.0	43200.0	449.381
	4	12	0.7710	0.6370	4880.5	8800.0	50400.0	488.479
	5	8	0.9689	0.8065	4355.4	8000.0	45000.0	435.888
	5	10	0.7853	0.7042	4673.3	9500.0	54000.0	467.774
	5	12	0.7744	0.6415	5062.1	11000.0	63000.0	506.767
PNU	4	8	0.9873	0.9287	5187.2	6400.0	36000.0	519.052
	4	10	0.9928	0.8337	4969.6	7600.0	43200.0	497.338
	4	12	0.9370	0.7730	5372.8	8800.0	50400.0	537.752
	5	8	0.9873	0.9437	5316.2	8000.0	45000.0	532.045
	5	10	0.9945	0.8664	5545.3	9500.0	54000.0	555.057
	5	12	0.9612	0.7970	5626.3	11000.0	63000.0	563.249

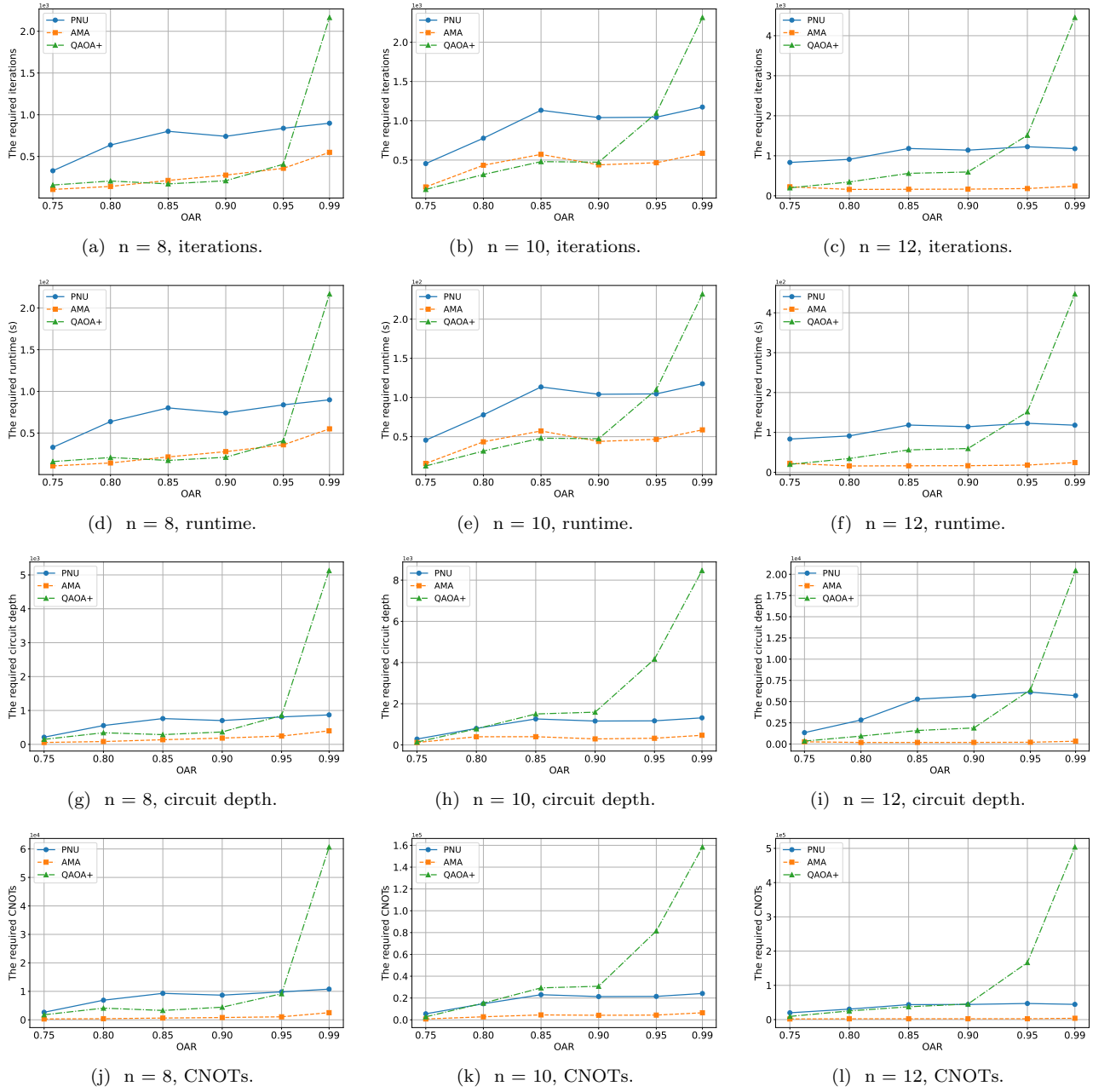


FIG. A1: The total resources (i.e., iterations, runtime, circuit depth, and CNOT gates) consumed by different algorithms to achieve the given OAR on ER graphs with varying graph sizes  $n$ .

trend further emphasizes the advantages of the AMA algorithm under high OAR requirements, demonstrating that at the same OAR, AMA not only significantly reduces runtime and iteration counts, but also effectively lowers circuit depth and the number of CNOT gates, thereby exhibiting higher computational efficiency and resource savings.

Further analysis reveals that the efficiency of AMA is demonstrated through its resource utilization during the optimization process. Particularly in scenarios with

high OAR requirements, AMA can converge to a quasi-optimal solution with relatively low computational resource consumption. This characteristic makes AMA highly competitive and applicable to real-world problems that demand high precision and large computational resources. These numerical simulation results not only verify the superior performance of AMA but also confirm its adaptability and robustness when faced with varying OAR requirements. This highlights its potential as an efficient algorithm, especially in resource-constrained application scenarios such as quantum computing, where the AMA algorithm offers significant practical value.

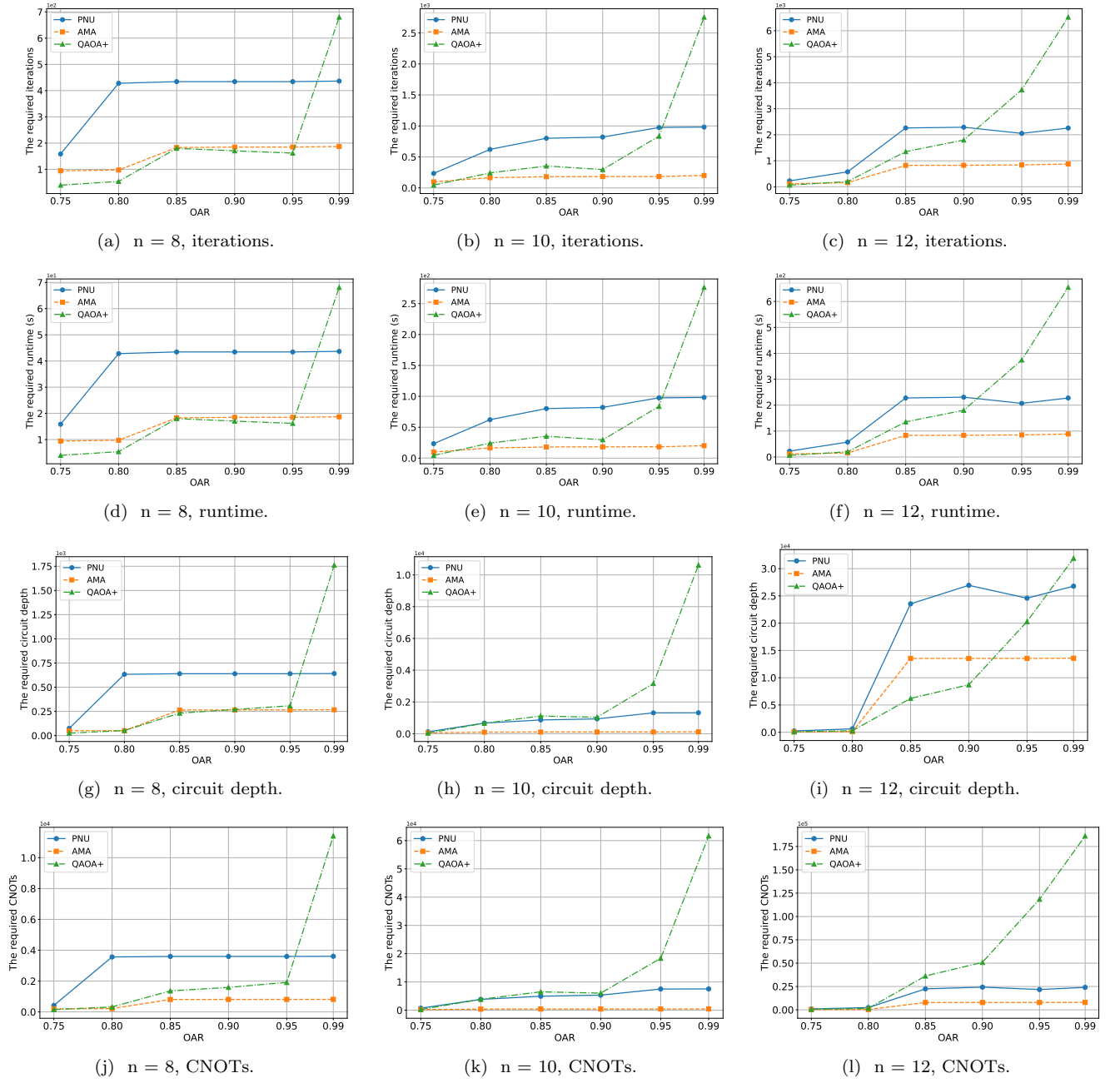


FIG. A2: The total resources (i.e., iterations, runtime, circuit depth, and CNOT gates) consumed by different algorithms to achieve the given OAR on 3-regular graphs with varying graph sizes  $n$